Physical Properties of the Noncentrosymmetric Superconductor $Mg_{10}Ir_{19}B_{16}$

T. Klimczuk,[1,2] F. Ronning,[1] V. Sidorov,[1,3] R. J. Cava,[4] and J. D. Thompson[1]

[1]*Condensed Matter and Thermal Physics, Los Alamos National Laboratory, Los Alamos, New Mexico 87545, USA*
[2]*Faculty of Applied Physics, Gdansk University of Technology, Narutowicza 11/12, 80-952 Gdansk, Poland*
[3]*Vereshchagin Institute for High Pressure Physics, Russian Academy of Sciences, 142190 Troitsk, Russia*
[4]*Department of Chemistry, Princeton University, Princeton New Jersey 08544, USA*

(Received 14 June 2007; published 19 December 2007)

Specific heat, electrical resistivity, and magnetic susceptibility measurements on a high quality sample of $Mg_{10}Ir_{19}B_{16}$ provide a self-consistent determination of its superconducting properties. They indicate that $Mg_{10}Ir_{19}B_{16}$ is a type-II superconductor [$T_C = 4.45$ K, $\kappa(0) \approx 20$], with an electron-phonon coupling constant $\lambda_{ep} = 0.66$. An analysis of the T-dependent specific heat shows that superconducting properties are dominated by an s-wave gap ($\Delta = 0.7$ meV). Point contact tunneling data provide evidence for multiple superconducting gaps, as expected from strong asymmetric spin-orbit coupling.

DOI: 10.1103/PhysRevLett.99.257004 PACS numbers: 74.70.Dd, 74.25.Bt, 75.40.Cx

The discovery of superconductivity in $CePt_3Si$ [1] has stimulated theoretical and experimental efforts to understand the role of the lack of crystal-structure inversion symmetry on superconductivity. Noncentrosymmetric heavy fermion superconductors [1–4] have attracted the most attention due to the unconventional behavior observed in these strongly correlated electron compounds. However, transition-metal compounds such as Li_2M_3B (M = Pd and Pt) [5,6], $Mg_{10}Ir_{19}B_{16}$ [7], and M_2Ga_9 (M = Rh, Ir) [8] are more straightforward for exploring the basic effects derived from breaking inversion symmetry. The asymmetric spin-orbit coupling (SOC) in noncentrosymmetric compounds leads to breaking parity conservation and, therefore, the strength of the SOC, which is determined by the crystallographic structure and elemental composition, has a nontrivial effect on the symmetry of Cooper pairs [9–11]. NMR [12] and magnetic penetration depth [13] measurements on Li_2M_3B highlight the role of composition: increasing SOC by replacing Pd with Pt changes the superconducting order parameter from dominantly spin-singlet (Li_2Pd_3B) to nodal, spin-triplet (Li_2Pt_3B).

$Mg_{10}Ir_{19}B_{16}$ crystallizes in a large ($a = 10.5668$ Å, I-43m), rather complex structure whose atomic positions are given in Ref. [7] and will be discussed elsewhere [14] in more detail. The noncentrosymmetry in $Mg_{10}Ir_{19}B_{16}$ is global, coming from Ir3 (24g site), Mg1 (8c site), and both B atoms (8c and 24g sites). Because Ir is a heavy transition metal, SOC is expected to have a significant influence on the properties, as Pt does in Li_2Pt_3B. We find that the thermodynamics of $Mg_{10}Ir_{19}B_{16}$ can be satisfactorily described with a conventional s-wave gap, while tunneling data present evidence for multiple gaps.

$Mg_{10}Ir_{19}B_{16}$ samples were synthesized by standard solid state reaction of pure Mg, Ir, and B elements as described in Ref. [7], with one important exception. The last heating was performed in a sealed Ta tube for 100 h at 850 °C. The sample purity was confirmed by powder x-ray diffraction using Cu $K\alpha$ radiation on a diffractometer; no extraneous second phases could be detected at the 5% level. Synthesis in a Ta tube allows heating the material for relatively long periods, which drastically improves chemical purity in comparison to the previous method [7].

Measurements of the dc magnetic susceptibility in a SQUID magnetometer (MPMS Quantum Design) showed that $Mg_{10}Ir_{19}B_{16}$ exhibits a temperature-independent Pauli susceptibility above ~100 K, below which there is a Curie-like tail that increases $\chi(T)$ by about 30% at 2 K [15]. The temperature dependence of the zero-field-cooled and field-cooled magnetic susceptibility in a field of 10 Oe is plotted in the inset of Fig. 1(a). The superconducting transition temperature found in these measurements is $T_{C\,\mathrm{onset}} = 4.4$ K, which is close to the previous report [7]. At 2 K, the diamagnetic response, after demagnetization correction, is about $0.95(1/4\pi)$. The much lower field-cooled signal is an indication of a substantial pinning effect, possibly on grain boundaries, that is reflected as well in $M(H)$ hysteresis (not shown).

The heat capacity was measured using an adiabatic relaxation calorimeter (Quantum Design PPMS). Figure 1(a) shows C/T versus T^2 in the temperature range 0.4–7.5 K in different magnetic fields. The bulk nature of the superconductivity and good quality of the sample are confirmed by a sharp anomaly at $T_C = 4.45$ K which is consistent with $T_{C\,\mathrm{onset}}$ determined by $\chi(T)$. In zero field a small but clear residual linear term $\gamma_0 = 2.5$ mJ/mol K^2 is observed in the $T \to 0$ K limit (see also Fig. 2 inset). While γ_0 could originate from a nodal superconducting gap provided that the impurity bandwidth is sufficiently large, we attribute it more likely to a small fraction of nonsuperconducting impurity phases. The measurement at $\mu_0 H = 5$ T, which exceeds H_{C2}, was fitted using the formula $C = \gamma T + \beta T^3 + \delta T^5$ and gives the parameters $\gamma = 55.1(1)$ mJ/mol K^2, $\beta = 3.97(1)$ mJ/mol K^4, and $\delta = 7.4(2)$ μJ/mol K^6. The first and last two terms are attributed to the electronic and lattice contribution to the heat capacity, respectively. By subtracting the impurity concentration γ_0 we find the Sommerfeld coefficient for $Mg_{10}Ir_{19}B_{16}$ $\gamma_n = \gamma - \gamma_0 = 52.6$ mJ/mol K^2. Knowing

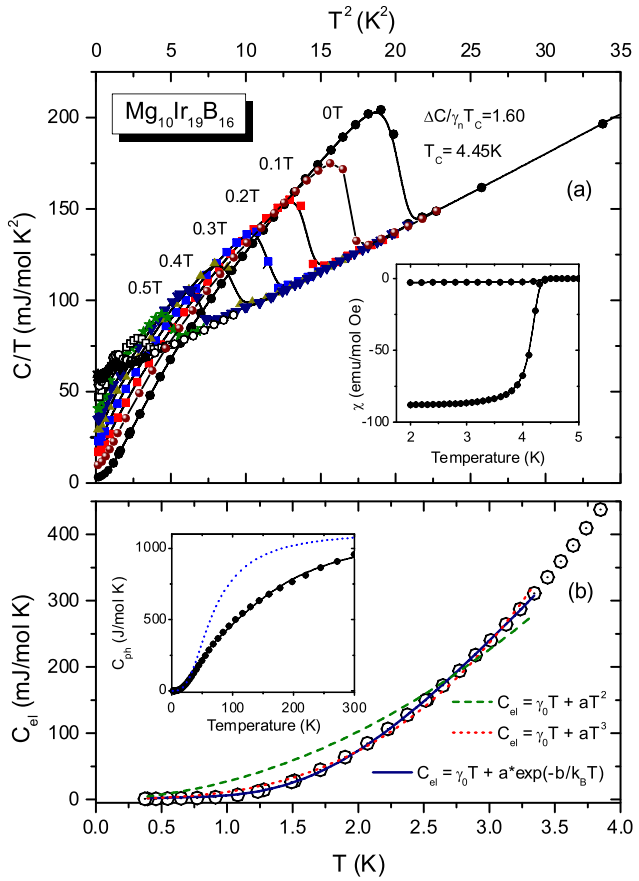

FIG. 1 (color online). (a) Specific heat divided by temperature (C/T) as a function of T^2 under magnetic field from 0 to 1 T increasing by steps of $\Delta\mu_0 H = 0.1$ T. The inset shows the superconducting transition measured in zero-field-cooled and field-cooled mode. (b) Temperature dependent electronic contribution to the specific heat of $Mg_{10}Ir_{19}B_{16}$. Lines are fits described in the text. The inset shows lattice specific heat (C_{ph}) as a function of temperature from 2 to 300 K. The blue dotted line represents a Debye model expectation ($\Theta_D = 280$ K) and black solid line is a fit to a Debye model ($\Theta_D = 740$ K) plus an Einstein mode fit ($\Theta_D = 147$ K). See text for details.

γ_n we can calculate the normalized specific heat jump, $\Delta C/\gamma_n T_C = 1.60$, which suggests an enhanced electron-phonon coupling. In a simple Debye model for the phonon contribution, the β coefficient is related to the Debye temperature (Θ_D) through $\Theta_D = (\frac{12\pi^4}{5\beta} nR)^{1/3}$, where $R = 8.314$ J/mol K and $n = 45$ for $Mg_{10}Ir_{19}B_{16}$. However, a $\Theta_D = 280$ K derived from this relation strongly overestimates the heat capacity between 10 and 300 K as shown in the inset of Fig. 1(b). This indicates that a simple Debye model that accurately models the acoustic modes at low energies fails to capture the higher energy optical modes that must be present in this material. To estimate the role of optical phonons, we fit the data above 10 K to a Debye model plus an Einstein mode, as was done for MgB_2 [16]. The fit gives 63% of the weight to a Debye term with $\Theta_D = 740$ K, and the remaining weight in an Einstein mode with energy $\Theta_E = 147$ K.

The electron-phonon coupling constant (λ_{ep}) can be estimated from the modified McMillian formula [17,18]: $\lambda_{ep} = [1.04 + \mu^* \ln(\omega_{log}/1.2T_C)]/[(1 - 0.62\mu^*) \times \ln(\omega_{log}/1.2T_C) - 1.04]$, where μ^* is a Coulomb repulsion constant and ω_{log} is a logarithmic averaged phonon frequency and can be determined from $\Delta C/\gamma T_C|_{T_C} = 1.43[1 + 53(T_C/\omega_{log})^2 \ln(\omega_{log}/3T_C)]$. Taking $\mu^* = 0.10$, we determined $\omega_{log} = 145$ K and $\lambda_{ep} = 0.66$. This value suggests that $Mg_{10}Ir_{19}B_{16}$ is a moderate-coupling superconductor [19].

The temperature dependence of the electronic specific heat (C_{el}) below T_C is shown in Fig. 1(b). Three models were used to fit the data, $C \propto T^2$, T^3, and $e^{-b/kT}$, expected for line nodes, point nodes, and a conventional, fully gapped model, respectively. The small residual linear term ($\gamma_0 T$) of $2.5^* T$ (mJ/mol K) was held constant throughout the fits. The best fit is provided by a fully gapped mode. An s-wave BCS model of the entire $C_{es}(0\text{ T})$ data gives $2\Delta_0 = 1.4$ meV or 16 K, comparable to the energy gap in Li_2Pt_3B (7.7 K) and Li_2Pd_3B (29.6 K) [20].

Dominance of an s-wave channel is supported by measurements of the magnetic field dependence of the Sommerfeld parameter $\gamma(H)$. For a highly anisotropic gap or a gap with nodes, theory predicts a nonlinear $\gamma(H) \propto H^{1/2}$ dependence [21]. In contrast, for a fully gapped superconductor, $\gamma(H)$ should be proportional to the number of field-induced vortices, i.e., $\gamma(H) \propto H$. As shown in Fig. 2, the field-linear increase in $\gamma(H)$ suggests that most electronic states near the Fermi energy are gapped in $Mg_{10}Ir_{19}B_{16}$ and clearly is at odds with a $\gamma(H) \propto H^{1/2}$ dependence.

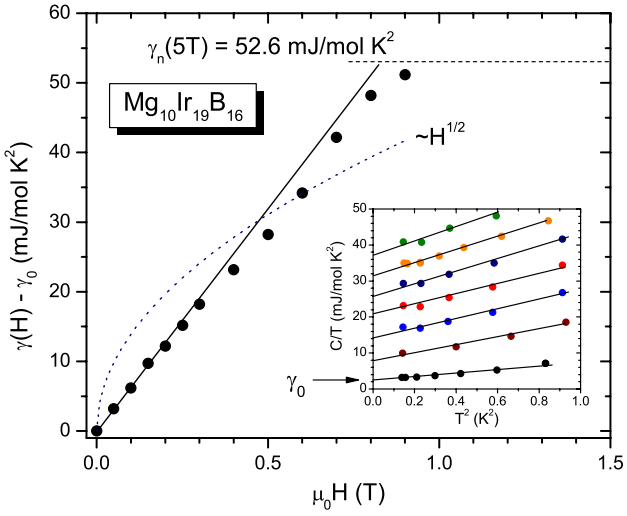

FIG. 2 (color online). Magnetic field dependence of $\gamma(H)$ as a function of magnetic field $\mu_0 H$. The solid (black) line corresponds to a linear ($\sim H$) relation and dotted (blue) line represents the nonlinear ($\sim H^{1/2}$) relation. The inset shows C/T vs T^2 under magnetic field (0–0.6 T) in the lowest temperature region.

In Fig. 3, the resistively determined upper critical field (Fig. 3 inset) and that obtained from specific heat measurements (see Fig. 1) coincide within experimental uncertainty at low fields but diverge with increasing field. As the magnetic field is raised, the resistive transition width increases from 0.1 to 0.8 K for fields of 0 and 1.2 T, respectively. One interpretation of the transition broadening is that it arises from filamentarylike superconductivity along grain boundaries, where scattering is stronger. The associated reduced electronic mean free path, in turn, would decrease the intrinsic coherence length and raise the resistive H_{C2} relative to the bulk H_{C2} determined by specific heat, which we take to be intrinsic. As shown by the dashed line in Fig. 3, the temperature dependence of $H_{C2}(T)$ is described by the Werthamer-Helfand-Hohenberg (WHH) [22] expression for a dirty type-II superconductor and gives $\mu_0 H_{C2}^{\mathrm{WHH}}(0) = 0.77(2)T$, consistent with results

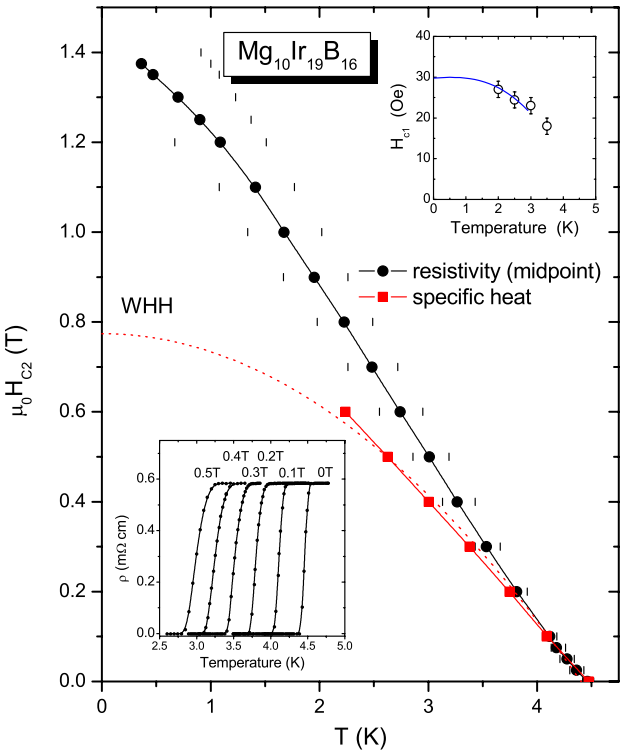

FIG. 3 (color online). The upper critical field ($\mu_0 H_{C2}$) from specific heat (red squares) and from resistivity (black circles) as a function of temperature. The vertical bars show 5% and 95% of the resistively determined superconducting transition. The dashed curve is predicted by the WHH expression. The upper right inset is the temperature dependence of the lower critical field ($\mu_0 H_{C1}$) for $Mg_{10}Ir_{19}B_{16}$. The lower left inset shows the resistivity near T_C for representative applied fields. From the initial slope $-dH_{C2}/dT_C = 2700$ Oe/K (using specific heat data), $\gamma = 52.6$ mJ/mol K^2, and the relation $\frac{dH_{C2}}{dT}|_{T_C} = 4.48 \times 10^4 \gamma\rho$ (Oe/K) (with γ in erg/cm^3 K^2 and ρ in Ω cm), we estimate the intrinsic intragranular resistivity $\rho(T \geq T_C) \approx 80\ \mu\Omega$ cm. This intragranular resistivity is only about 14% of the value seen in the inset, consistent with strong intergranular scattering and an associated larger H_{C2} measured resistively.

in Fig. 3. This value of $H_{c2}(0)$ for $Mg_{10}Ir_{19}B_{16}$ is smaller than previously reported [7]; however, the purity of the present sample is much better, resulting in a longer mean path, and the earlier result was based only on resistivity measurements which we have found can lead to a much higher $H_{C2}(0)$. Assuming a Landé g factor of 2, the measured $H_{C2}(0)$ is well below the weak-coupling Pauli field of ≈ 8.2 T, indicating that the observed critical field is dominated by orbital pair-breaking.

The lower critical field values, $H_{C1}(T)$, were determined from low-field $M(H)$ curves in which special care was taken to correct for a small residual trapped field in the superconducting magnet and for demagnetization effects. With these precautions, $H_{C1}(T)$ was defined as the field at which $M(H)$ deviated by 1% from a perfect diamagnetic response. Values are plotted in the inset of Fig. 3, and their extrapolation to $T = 0$ K gives $\mu_0 H_{C1}(0) = 3$ mT.

With these results for $H_{C1}(0)$ and $H_{C2}(0)$, we can estimate several superconducting parameters for $Mg_{10}Ir_{19}B_{16}$. From $\mu_0 H_{C2} = \Phi_0/2\pi\xi_{\mathrm{GL}}^2$, where Φ_0 is the quantum flux ($h/2e$), we find a Ginzburg-Landau coherence length $\xi_{\mathrm{GL}}(0) = 206$ Å. Knowing $\xi_{\mathrm{GL}}(0)$ and $H_{C1}(0)$, a penetration depth, $\lambda_{\mathrm{GL}}(0) = 4040$ Å, is obtained from $\mu_0 H_{C1} = (\Phi_0/4\pi\lambda_{\mathrm{GL}}^2)\ln(\lambda_{\mathrm{GL}}/\xi_{\mathrm{GL}})$, and, hence, the Ginzburg-Landau parameter, $\kappa(0) \approx 20$. Using these parameters and the relation $H_{C1}H_{C2} = H_C^2 \ln(\kappa)$, we find that the thermodynamic critical field $\mu_0 H_C(0) = 28$ mT. The superconducting condensation energy provides a stringent self-consistency check on the derived parameters. The condensation energy relates the thermodynamic critical field to measured specific heat difference between zero field and the normal state through $\mu_0 H_C^2(0)/2 = F_N - F_S = \iint (C(5\,\mathrm{T}) - C(0\,\mathrm{T}))/T dT$. This method of calculating the thermodynamic critical field gives $\mu_0 H_C(0) = 30$ mT, in excellent agreement with $\mu_0 H_C(0)$ determined by the critical fields. In addition, the condensation energy is related to the density of states and the gap value by $\mu_0 H_C^2(0) = N(E_F)(1 + \lambda_{\mathrm{ep}})\Delta_0^2$. We obtain $N(E_F)(1 + \lambda_{\mathrm{ep}})$ from γ_n and calculate Δ_0 to be 0.62 meV, which agrees very well with the value of 0.7 meV obtained directly from a fit to the zero field specific heat.

While a single s-wave gap is indicated by transport and thermodynamic measurements, we obtain a different view from point contact spectroscopy measurements [23]. A representative normalized conductance curve is shown in Fig. 4. Multiple energy scales are observed as marked by the arrows. Tracking the temperature dependence of these energy scales (inset of Fig. 4) shows that both correlate well with the BCS gap expectation, and it also shows that we are not in the thermal regime which would give a $(1 - (T/T_C)^2)^{1/2}$ dependence. Furthermore, a simple fit assuming pure Andreev reflection from a multiband superconductor with two gaps (solid line) gives values of 0.56 and 2.2 meV. We note that the more dominant lower energy scale is in reasonable agreement with the gap obtained by our thermodynamic measurements, but that a single gap fit

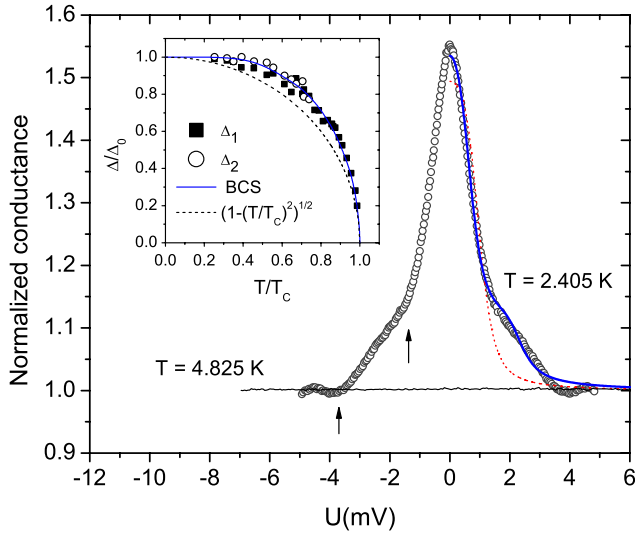

FIG. 4 (color online). Normalized conductance spectra at 2.405 K (circles) and 4.825 K $> T_C$ (thin black line). Arrows indicate the presence of two energy scales in the superconducting state. The dashed (solid) line is a fit assuming pure Andreev reflection with one (two) gap(s). Relaxing this assumption within the Blonder-Tinkham-Klapwijk formalism did not improve the fits. The inset shows the temperature dependence of the two gap scales compared with theoretical expectations.

(dashed line) giving $\Delta = 0.84$ meV cannot capture the shoulder above 1 meV.

The observation of multiple gaps is as expected, due to the mixing of the spin-singlet and spin-triplet order parameters. However, no conclusive evidence for such physics was observed by our other measurements. We could speculate that the larger gap would manifest itself most strongly in the specific heat data near T_C, but that inhomogeneity may blur the features. Perhaps, due to the local nature of the probe, point contact tunneling can more easily resolve multiple gap features. A more detailed theory is needed to analyze the complete set of data to extract the full multigap structure, and measurements on single crystals would be useful in resolving the apparent discrepancy between thermodynamic and tunneling measurements.

In summary, a self-consistent set of superconducting and normal state parameters confirm the validity of measured and derived properties from a high quality sample of $Mg_{10}Ir_{19}B_{16}$ and provide a benchmark for refined band structure calculations that explicitly include the effect of SOC that must be present. Asymmetric spin-orbit coupling arising from the heavy element Ir should spin-split degenerate electronic bands by a factor many times $k_B T_C$, and, therefore, allow mixing of spin-singlet and spin-triplet pairing states [10]. A single band with a gap of 0.7 meV can account for the large majority of the data. In contrast, we find clear evidence for multiple gaps from tunneling measurements. Nuclear spin-lattice relaxation and Knight-shift measurements on ideally purer samples should reveal unambiguously the presence or absence of a nodal gap structure and the existence of a spin-triplet component in the superconducting state.

We thank H. Q. Yuan for useful discussions. Work at Los Alamos and Princeton was performed under the auspices of the U.S. DOE, Office of Science.

Note added.—Upon completion of this work we became aware of a similar characterization analysis of Ref. [24], which has similar conclusions as our thermodynamic measurements.

[1] E. Bauer *et al.*, Phys. Rev. Lett. **92**, 027003 (2004).
[2] T. Akazawa *et al.*, J. Phys. Soc. Jpn. **73**, 3129 (2004).
[3] N. Kimura *et al.*, Phys. Rev. Lett. **95**, 247004 (2005).
[4] I. Sugitani *et al.*, J. Phys. Soc. Jpn. **75**, 043703 (2006).
[5] K. Togano *et al.*, Phys. Rev. Lett. **93**, 247004 (2004).
[6] P. Badica, T. Kondo, and K. Togano, J. Phys. Soc. Jpn. **74**, 1014 (2005).
[7] T. Klimczuk *et al.*, Phys. Rev. B **74**, 220502 (2006).
[8] T. Shibayama *et al.*, J. Phys. Soc. Jpn. **76**, 073708 (2007).
[9] K. V. Samokhin, E. S. Zijlstra, and S. K. Bose, Phys. Rev. B **69**, 094514 (2004).
[10] P. A. Frigeri, D. F. Agterberg, A. Koga, and M. Sigrist, Phys. Rev. Lett. **92**, 097001 (2004).
[11] M. Sigrist *et al.*, J. Magn. Magn. Mater. **310**, 536 (2007).
[12] M. Nishiyama, Y. Inada, and Guo-qing Zheng, Phys. Rev. Lett. **98**, 047002 (2007).
[13] H. Q. Yuan *et al.*, Phys. Rev. Lett. **97**, 017006 (2006).
[14] Q. Xu *et al.* (unpublished).
[15] The measured, temperature-independent susceptibility above ~100 K is weakly diamagnetic, $\chi = -4.5e^{-4}$ emu/mol. Correcting the measured χ for core diamagnetic contributions ($\chi_c = -7e^{-4}$ emu/mol) gives a Pauli susceptibility of $2.5e^{-4}$ emu/mol. Assuming a Wilson ratio of 1 and taking values of the Sommerfeld coefficient and electron-phonon coupling parameter, discussed in the text, the calculated Pauli susceptibility is $4.4e^{-4}$ emu/mol, in reasonable agreement with the estimate above.
[16] Ch. Wälti *et al.*, Phys. Rev. B **64**, 172515 (2001).
[17] P. B. Allen and R. C. Dynes, Phys. Rev. B **12**, 905 (1975).
[18] J. P. Carbotte, Rev. Mod. Phys. **62**, 1027 (1990).
[19] Band structure calculations, which neglect spin-orbit coupling find the density of states 11.03 states/eV f.u. (B. Wiendlocha *et al.*, arXiv:07004.1295). Taking that value in the equation $N(E_F) = 2\frac{3\gamma_n}{2\pi^2 k_B^2(1+\lambda_{ph})}$, we find the electron-phonon coupling $\lambda_{ph} = 1.02$; however, λ_{ph} determined here relies on the validity of the band structure calculation without SOC and should be taken with caution.
[20] H. Takeya *et al.*, Phys. Rev. B **72**, 104506 (2005).
[21] G. E. Volovik, JETP Lett. **58**, 469 (1993).
[22] N. R. Werthamer, E. Helfand, and P. C. Hohenberg, Phys. Rev. **147**, 295 (1966).
[23] V. Sidorov *et al.* (unpublished); Thermally reproducible contacts ($R \sim 15\ \Omega$) were made with silver paint as in R. S. Gonnelli *et al.*, Phys. Rev. Lett. **89**, 247004 (2002).
[24] Gang Mu, Yue Wang, Lei Shan, and Hai-Hu Wen, Phys. Rev. B **76**, 064527 (2007).